The Theoretical Flow Ripple of an External Gear Pump

Noah D. Manring
Mechanical and Aerospace Engineering Department,
University of Missouri–Columbia,
Columbia, MO 65211

Suresh B. Kasaragadda
Mechanical and Aerospace Engineering Department,
University of Missouri–Columbia,
Columbia, MO 65211

In this paper, the theoretical flow ripple of an external gear pump is studied for pumps of similar size using different numbers of teeth on the driving and driven gears. In this work, the flow ripple equation is derived based upon the flow of incompressible fluid across the changing boundaries of a control volume. From this method, it is shown that the instantaneous length of action within the gear mesh determines the instantaneous flow ripple. A numerical and a closed-form approximation are presented for the instantaneous length of action and it is shown that the difference between these two solutions is negligible. Fast Fourier transform analysis is employed for identifying the harmonic frequencies and amplitudes of the flow pulse and these results are compared for 16 different pump designs. In summary, the results of this study show that the driving gear dictates the flow ripple characteristics of the pump while the driven gear dictates the pump size. As a result, it may be advantageous to design an external gear pump with a large number of teeth on the driving gear and a fewer number of teeth on the driven gear. This design configuration will tend to reduce both the physical pump size (without reducing the volumetric displacement of the pump) and the amplitude of the flow pulsation, while increasing the natural harmonic frequencies of the machine. [DOI: 10.1115/1.1592193]

Introduction

Background. Hydraulic pumps are the power-supplying components within hydraulic circuitry. All pumps used in hydrostatic pressure systems are of the positive displacement type. Non-positive displacement pumps, usually characterized by the features of low pressure and high flow rate, are incapable of producing sufficient power required by the hydrostatic power systems. Among the positive displacement pumps, fixed displacement gear pumps are often used in circuit applications where customers are sensitive to the initial purchase cost of the system and where the overall operating efficiency does not need to be extremely high. Also, gear pumps can be operated at high speeds and can be used in applications where the operating pressures are low to moderate. Gear pumps use a very simple mechanism to generate flow, and therefore have a minimum number of parts associated with the design. The simplicity of the gear pump design translates into higher reliability as compared to other positive displacement pumps that use a more complex design.

Though gear pumps enjoy a high level of reliability and offer a low purchase cost to the end customer, they are often accompanied with performance characteristics that tend to create higher noise levels than other types of positive displacement pumps. These noise levels are associated with the substantial flow ripple of the pump, which induces a pressure ripple and oscillating forces within the system. Since the flow ripple is considered to be the first cause of these oscillating forces, it is assumed that a smoother flow delivery of the pump will also attenuate the noise that is generated. This paper is focused on considering the characteristics of the flow ripple from an ideal, or theoretical, point of view.

Literature Review. Gear pumps are among the oldest and most commonly used pumps within the industry. Though the gear pump is extremely simple in its operating principle, the fundamental understanding of the instantaneous pump flow has been a subject of considerable interest for many years. The complexity of this subject arises due to the nature of the geometry involved, which has typically required numerical analysis to solve the governing equations. Much of the recent research that is most germane to gear pump technology is briefly summarized in the following paragraph.

Research pertaining to the average flow rate of the gear pump has been conducted by Frith and Scott [1]. In their work, the authors have related the degradation of the average flow rate to the online generation of wear debris. In other research, authors have emphasized a prediction in the fluid film thickness between the gear end-face and the end wear-plate [2–4]. In this work, the authors were primarily concerned with volumetric leakage and pump efficiency. For predicting the cyclic moments and forces on the pump shaft, Foster, Taylor, and Bidhendi [5] conducted an in-depth analysis of the gear pump using a computer program for generating solutions. This work considered the trapped volume of fluid between meshing teeth and the results were shown to compare nicely with actual test data. Still, others have focused on various tooth geometries in an effort to reduce and/or compare the discharge flow amplitude of the pump [6,7].

Though all of this work has been valuable in and of itself, none of this work has considered a comparison of same-size external gear pumps, which use different numbers of teeth for the driving and driven gears. The question related to tooth number is significant since other positive-displacement pump types tend to exhibit different flow characteristics depending upon the number of discrete pumping elements that are used. For instance, axial piston pumps have been shown to exhibit significantly different pulse shapes for pumps that use an even versus an odd number of pistons [8]. This present study is aimed at documenting the theoretical effects of altering the tooth number on the gears that are used within external gear pump designs.

Research Objectives. The primary objective of this research is to study the flow ripple of an external gear pump as it varies using different combinations of teeth for the driving and driven gear. By conducting this study, it is expected that generalized conclusions will be made regarding the impact of using different numbers of gear teeth within pumps of similar size. As noted in the literature review, a study of this type has not yet been published.

This research begins by nondimensionalizing the variables that will be used in the analysis. The motivation for conducting non-

Contributed by the Dynamic Systems, Meausrements, and Control Division of THE AMERICAN SOCIETY OF MECHANICAL ENGINEERS for publication in the ASME JOURNAL OF DYNAMIC SYSTEMS, MEASUREMENT, AND CONTROL. Manuscript received by the ASME Dynamics Systems and Control Division February 1, 2002; final revision, November 6, 2002. Associate Editor, A. Alleyne.

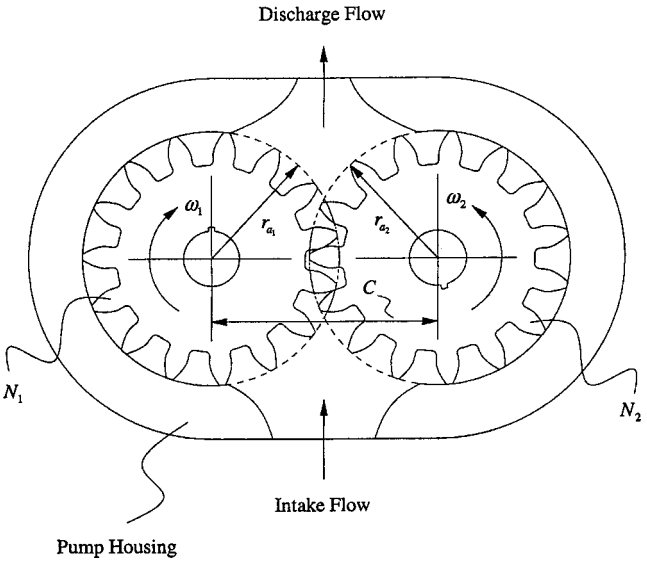

Fig. 1 Gear pump configuration

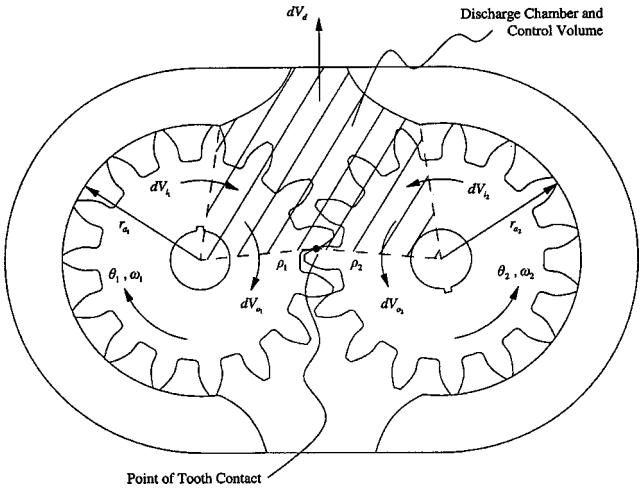

Fig. 2 Control volume of the discharge chamber

dimensional analysis is to make the results applicable for pumps of any size. This means that the final results can be simply scaled for a specific design situation. The second task of this research is to derive the governing equations for the flow ripple of the pump. This is done using a control volume approach and it is shown that the flow ripple equation is dependent upon the instantaneous length of action for the two teeth that instantaneously define the discharge chamber of the pump. Recognizing this, the third task of this research is to find a solution for the instantaneous length of action for the two contacting teeth. Both numerical and closed-form approximations for this parameter are sought. Finally, 16 different pumps are designed with the same average volumetric displacement but with different numbers of teeth on both the driving and the driven gears. The flow ripple characteristics of these pumps are systematically compared using fast Fourier transform (FFT) methods and generalized conclusions are drawn from these results.

Pump Description

Figure 1 shows a cross-sectional view taken through the gears of a typical gear pump. Note: like most actual gear pump designs, this pump is shown with two identical gears that are used for displacing fluid. In the analysis that follows, the numbers of teeth on each gear will be allowed to vary and therefore, in general, the two gears will not be identical. The number of teeth on gear 1 is given by N_1 and the number of teeth on gear 2 is given by N_2. In any case, the addendum radius of each gear will be identified by the dimension $r_{a_{1,2}}$, the pitch radius is given by $r_{p_{1,2}}$, and the center distance between shafts is given by the dimension C. Note: the subscripts 1 and 2 denote the driving and driven gear respectively. The thickness of the gears into the paper is given by the dimension w (not shown in Fig. 1). The gears are contained in a close-tolerance housing that separates the discharge port from the intake port. An external shaft is connected to gear 1 while the other gear is supported by an internal shaft and bearing. Note: the shafts connected to the gears are not shown in Fig. 1 as they would protrude out of the paper. The driving gear and shaft rotate at an angular velocity ω_1. The driven gear rotates in the opposite direction at an angular velocity ω_2.

When considering the operation of a gear pump, it is a common mistake to assume that the fluid flow occurs through the center of the pump (i.e., through the meshed gear geometry). This is not what happens. To produce flow with a gear pump, fluid is carried around the *outside* of each gear (within each tooth gap) from the intake side of the pump to the discharge side of the pump. As the gear teeth mesh within the gearset, fluid is squeezed out of each tooth gap by a mating tooth and is thereby displaced into the discharge line of the pump. On the intake side, the gear teeth are coming out of the mesh. In this condition, fluid backfills for the volume of the mating teeth that are now evacuating each tooth space. This backfilling draws fluid into the pump through the intake port of the pump housing. This process repeats itself for each revolution of the pump and thereby displaces fluid at a rate proportional to the pump speed.

Dimensionless Variables

Before conducting this research, it is important to nondimensionalize the variables that will be used. Not only does this simplify the development of equations by eliminating various scale factors within each equation, but it also makes the results most general and useful to the end user of this research. By developing nondimensional equations, the results are applicable to gear pumps of any physical size. The final results may be simply scaled according to the rules that were used to nondimensionalize the specific quantity of interest. The dimensionless variables that will be used in this work are generally given as follows:

$$\hat{l}=\frac{l}{r_{b_1}},\quad \hat{r}=\frac{r}{r_{b_1}},\quad \hat{x}=\frac{x}{r_{b_1}},\quad \hat{y}=\frac{y}{r_{b_1}},\quad \hat{\rho}=\frac{\rho}{r_{b_1}},$$

$$\hat{Q}=\frac{Q}{w\omega_1 r_{b_1}^2},\quad \hat{t}=t\omega_1=\theta_1,\quad \hat{V}=\frac{V}{wr_{b_1}^2}, \tag{1}$$

where all symbols are defined in the Nomenclature section of this paper. Note: all dimensionless quantities throughout this paper will be identified by carets over the top. All length dimensions have been nondimensionalized using the radius of the base circle for the driving gear, r_{b_1}.

Pump Flow Analysis

In the following analysis, the ideal pump will be considered by assuming the following things: (1) the fluid is incompressible, (2) fluid leakage is neglected, and (3) the pump parts are rigid and inflexible. Figure 2 shows a crosshatched area that defines the discharge chamber of the gear pump. At a particular instant in time, the boundaries of this chamber define the control volume of interest. Since the fluid is incompressible, the total volume entering the discharge chamber must equal the total volume leaving the discharge chamber. Figure 2 shows infinitesimally small volumes that are crossing the boundaries of the control volume at a particular instant in time. Note: the material within these volumes is irrelevant since everything is considered to be incompressible, however, the infinitesimally small volumes generally consist of

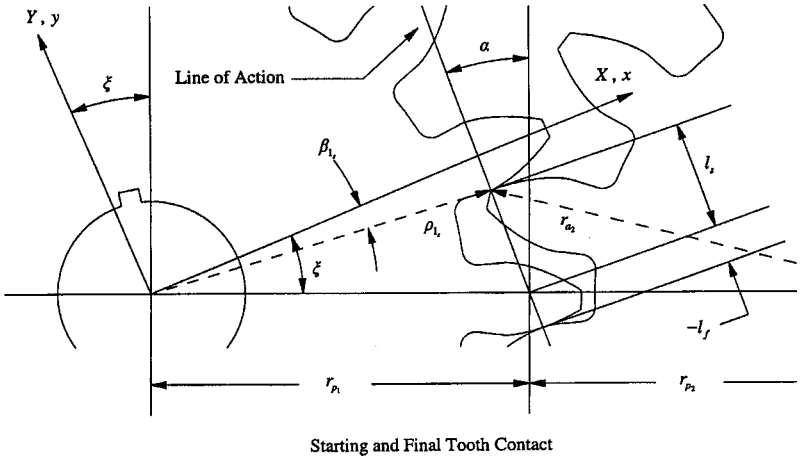

Fig. 3 Gear mesh geometry at the first point of tooth contact

both gear pump material (e.g., steel) and fluid. In Fig. 2, the input volume from the driving gear (i.e., gear 1) is given by dV_{i_1}, however, a certain amount of gear volume is also leaving the control volume. This exiting volume from gear 1 is given by dV_{o_1}. Similarly, the input and exiting volumes from gear 2 are given by dV_{i_2} and dV_{o_2}, respectively. Setting the input volumes equal to the output volumes yields the dimensionless governing equation for this problem:

$$d\hat{V}_d=(d\hat{V}_{i_1}-d\hat{V}_{o_1})+(d\hat{V}_{i_2}-d\hat{V}_{o_2}). \tag{2}$$

From geometry it can be shown that dimensionless expressions for the entering and exiting volumes are given by

$$d\hat{V}_{i_1}=\frac{1}{2}\hat{r}_{a_1}^2 d\theta_1, \quad d\hat{V}_{o_1}=\frac{1}{2}\hat{\rho}_1^2 d\theta_1,$$

$$d\hat{V}_{i_2}=\frac{1}{2}\hat{r}_{a_2}^2 d\theta_2, \quad d\hat{V}_{o_2}=\frac{1}{2}\hat{\rho}_2^2 d\theta_2, \tag{3}$$

where $r_{a_{1,2}}$ is the addendum radius, $\rho_{1,2}$ is the contact radius between the two sealing teeth in the mesh, and $\theta_{1,2}$ is the angle of rotation. Note: in Eq. (3), the subscripts, 1 and 2, denote the driving gear and driven gear, respectively. From the fundamental law of gearing, we know that

$$d\theta_2=\frac{\hat{r}_{p_1}}{\hat{r}_{p_2}}d\theta_1, \tag{4}$$

where $r_{p_{1,2}}$ is the pitch radius. Substituting Eqs. (3) and (4) into Eq. (2), and dividing the result by an infinitesimal amount of time dt, yields the following dimensionless result for the theoretical flow rate of the gear pump:

$$\hat{Q}_d=\frac{d\hat{V}_d}{d\hat{t}}=\frac{1}{2}\left\{(\hat{r}_{a_1}^2-\hat{\rho}_1^2)+\frac{\hat{r}_{p_1}}{\hat{r}_{p_2}}(\hat{r}_{a_2}^2-\hat{\rho}_2^2)\right\}. \tag{5}$$

As shown in Eq. (5), the instantaneous radii of tooth contact, ρ_1 and ρ_2, must be determined to evaluate the theoretical discharge flow of the pump. Using the law of cosines, and the geometry of Fig. 4 (to be discussed later), it can be shown that the instantaneous radii of tooth contact between the two meshing gears is given by

$$\hat{\rho}_1^2=\hat{l}^2+\hat{r}_{p_1}^2-2\hat{r}_{p_1}\hat{l}\sin(\alpha), \quad \hat{\rho}_2^2=\hat{l}^2+\hat{r}_{p_2}^2+2\hat{r}_{p_2}\hat{l}\sin(\alpha), \tag{6}$$

where α is the pressure angle and l is the instantaneous length of action shown in Fig. 4. Substituting Eq. (6) into Eq. (5) yields the following result for the instantaneous flow rate of the pump:

$$\hat{Q}_d=\frac{1}{2}\left\{\hat{r}_{a_1}^2+\hat{r}_{a_2}^2\frac{\hat{r}_{p_1}}{\hat{r}_{p_2}}-\hat{r}_{p_1}(\hat{r}_{p_1}+\hat{r}_{p_2})-\left(1+\frac{\hat{r}_{p_1}}{\hat{r}_{p_2}}\right)\hat{l}^2\right\}. \tag{7}$$

Results very similar to this have also been reported in previous literature [5,9]. Using this equation, the instantaneous flow rate of the pump may be determined once the instantaneous length of action, l, is known. The length of action can be determined from the mesh geometry of the gear.

Mesh Geometry

Coordinate Systems. Figures 3 and 4 show schematics of the gear mesh that occurs between two teeth that instantaneously define the control volume of the discharge chamber. Figure 3 shows the first point of tooth contact between the teeth while Fig. 4 shows an intermediate point of tooth contact. In these schematics, two Cartesian coordinate systems are shown: (1) there is a fixed Cartesian coordinate system denoted by the large X-Y coordinates, and (2) there is a rotating Cartesian coordinate system denoted by the small x-y coordinates. The fixed X-Y coordinate system is oriented by the fixed angular dimension ξ (which will be determined later). The x axis of the small rotating x-y coordinate system is attached to the centerline of the gear tooth on gear 1 and moves with this gear tooth as it rotates with the angular dimension θ_1. By definition, $\theta_1=0$ when the large X-Y and the small x-y coordinate systems are coincident and when the meshing teeth first make contact.

Instantaneous Point of Tooth Contact. The instantaneous point of tooth contact must always lie somewhere on the line of action and is located with respect to the rotating x-y coordinate system by the polar coordinates ρ_1 and β_1. From Fig. 4, it may be shown that the equation for the line of action with respect to the rotating x-y coordinate system is

$$\hat{y}\sin(\alpha+\theta_1-\xi)=1-\hat{x}\cos(\alpha+\theta_1-\xi), \tag{8}$$

where it has been recognized from gear geometry that $r_{b_1}=r_{p_1}\cos(\alpha)$. At the point of tooth contact, it is clear from Fig. 4 that $x=\rho_1\cos(\beta_1)$ and $y=-\rho_1\sin(\beta_1)$. Substituting these expressions into Eq. (8) yields the following equation which describes the point of tooth contact in terms of ρ_1 and β_1:

$$\hat{\rho}_1=\sec(\alpha+\beta_1+\theta_1-\xi). \tag{9}$$

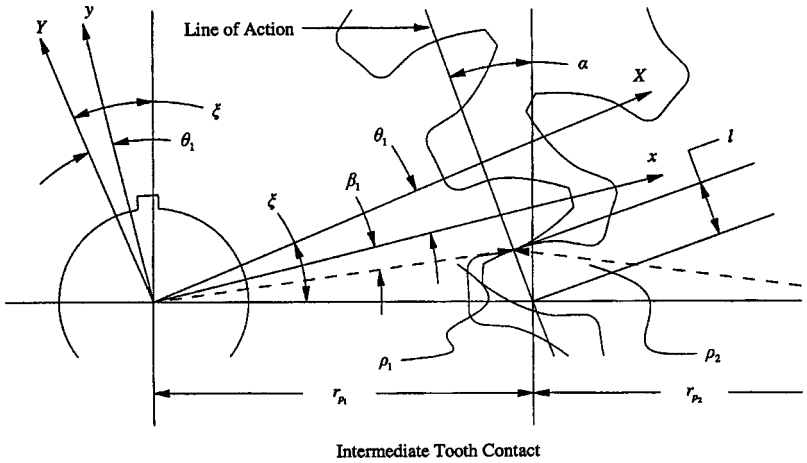

Fig. 4 Gear mesh geometry at an intermediate point of tooth contact

From the geometry of the involute tooth profile (see the Appendix) it may be shown that

$$\beta_1 = \psi_1 - \sqrt{\hat{\rho}_1^2 - 1} + \cos^{-1}\left(\frac{1}{\hat{\rho}_1}\right), \tag{10}$$

where $\psi_1 = \pi/(2N_1)$ and N_1 is the number of teeth on gear 1. Equations (9) and (10) must be solved numerically for a given rotational position θ_1. The numerical solution may then be used to describe the instantaneous point of tooth contact using the polar coordinates ρ_1 and β_1.

Starting Mesh Position. Figure 3 shows the starting position within the mesh when the gear teeth first make contact. This orientation of the gear mesh is a special case of the preceding analysis where the angular rotation of the driving gear is given by $\theta_1 = 0$. In this position, the two Cartesian coordinate systems (i.e., the large X-Y and small x-y coordinate systems) are coincident. The point of first contact between the gear teeth occurs when the tip of the driven gear (gear 2) first touches the surface profile of the driving gear (gear 1). In this position, it may be shown from geometry that

$$\hat{\rho}_{1_s} = \sqrt{\hat{l}_s^2 + \hat{r}_{p_1}^2 - 2\hat{r}_{p_1}\hat{l}_s \sin(\alpha)}, \tag{11}$$

where the starting length of action is given by

$$\hat{l}_s = \sqrt{\hat{r}_{a_2}^2 - \hat{r}_{p_2}^2 \cos^2(\alpha)} - \hat{r}_{p_2} \sin(\alpha). \tag{12}$$

Also, from the general form of Eq. (10), it may be shown that

$$\beta_{1_s} = \psi_1 - \sqrt{\hat{\rho}_{1_s}^2 - 1} + \cos^{-1}\left(\frac{1}{\hat{\rho}_{1_s}}\right). \tag{13}$$

In Eqs. (11)–(13), the subscript s is used to denote that these dimensions are given for the starting position only. From the geometry of Fig. 3, the angular dimension ξ, which orients the fixed X-Y coordinate system, may be determined as

$$\xi = \beta_{1_s} + \sin^{-1}\left(\frac{\hat{l}_s \cos(\alpha)}{\hat{\rho}_{1_s}}\right), \tag{14}$$

where ρ_{1_s}, l_s, and β_{1_s} are given in Eqs. (11)–(13), respectively.

Instantaneous Length of Action

Numerical Solutions. To determine the instantaneous pump flow, Eq. (7) must be used with the appropriate result for the instantaneous length of action, l. From the geometry of right triangles, and using Fig. 4, it can be shown that the instantaneous length of action is given by

$$\hat{l} = \hat{\rho}_1 \sin(\xi - \theta_1 - \beta_1)\sec(\alpha), \tag{15}$$

where ρ_1 and β_1 are given in Eqs. (9) and (10). The nonlinear relationship between ρ_1 and β_1 (see Eqs. (9) and (10)) requires a numerical solution for determining the instantaneous length of action according to Eq. (15). The numerical solution to these equations will yield the most accurate results possible; however, a closed-form approximation to these solutions would be more convenient to use.

Closed-Form Approximation. For generating a closed form solution for the instantaneous pump flow, a Taylor series expansion of Eq. (15) may be taken for small values of θ_1. This result is given by

$$\hat{l} = \hat{l}_s - \hat{\rho}_{1_s} \cos(\xi - \beta_{1_s})\sec(\alpha)\theta_1, \tag{16}$$

where l_s is given in Eq. (12), ρ_{1_s} is given in Eq. (11), β_{1_s} is given in Eq. (13), and ξ is given in Eq. (14). As it turns out, an even better approximation can be consistently made by assuming that $\hat{\rho}_{1_s}\cos(\xi - \beta_{1_s})\sec(\alpha) = 1$. Using this assumption, Eq. (16) may be written as

$$\hat{l} = \hat{l}_s - \theta_1, \tag{17}$$

where, again, $\hat{l}_s$ is given in Eq. (12). By subtracting Eq. (17) from the numerical solution of Eq. (15), an error associated with the approximation of Eq. (17) may be written as

$$\hat{\varepsilon} = \hat{\rho}_1 \sin(\xi - \theta_1 - \beta_1)\sec(\alpha) - \hat{l}_s + \theta_1. \tag{18}$$

This error is zero for $\theta_1 = 0$ but increases slightly as θ_1 gets larger. Numerical studies of this error have shown it to be negligible for the pump designs examined in this research.

Pump Flow Characteristics

The general form of Eq. (7) will be used to describe the flow characteristics of the pump. From Eq. (7), it can be shown that the maximum flow output of the pump will occur when l^2 is a minimum. For the case of each pump analyzed in this study, $\min(\hat{l}^2) = 0$. Therefore,

$$\hat{Q}_{d_{\max}} = \frac{1}{2}\left\{\hat{r}_{a_1}^2 + \hat{r}_{a_2}^2 \frac{\hat{r}_{p_1}}{\hat{r}_{p_2}} - \hat{r}_{p_1}(\hat{r}_{p_1} + \hat{r}_{p_2})\right\}. \tag{19}$$

Similarly, the minimum flow output of the pump will occur when l^2 is a maximum. Since $\max(\hat{l}^2) = \hat{l}_s^2$, the minimum pump flow rate is given by

Table 1 Pump designs with identical average flow rates ($\hat{Q}_d = 0.297$) and varying numbers of teeth on the driving and driven gears. The boldface row designs are shown in Fig. 5.

N_1	N_2	α	$\hat{r}_{p_1}$	$\hat{r}_{p_2}$	$\hat{r}_{a_1}$	$\hat{r}_{a_2}$	$\hat{l}_s$	$\hat{l}_f$
13	13	0.208	1.022	1.022	1.179	1.179	0.414	−0.075
13	14	0.214	1.023	1.102	1.181	1.259	0.419	−0.069
13	15	0.219	1.024	1.182	1.182	1.340	0.424	−0.065
13	**16**	**0.223**	**1.025**	**1.262**	**1.183**	**1.420**	**0.428**	**−0.060**
14	13	0.276	1.039	0.965	1.188	1.114	0.352	−0.097
14	14	0.280	1.041	1.041	1.189	1.189	0.356	−0.093
14	**15**	**0.283**	**1.042**	**1.116**	**1.190**	**1.265**	**0.360**	**−0.089**
14	16	0.286	1.042	1.191	1.191	1.340	0.364	−0.085
15	13	0.345	1.062	0.921	1.204	1.062	0.304	−0.115
15	**14**	**0.347**	**1.063**	**0.992**	**1.205**	**1.134**	**0.307**	**−0.112**
15	15	0.349	1.064	1.064	1.206	1.206	0.310	−0.109
15	16	0.351	1.065	1.136	1.207	1.278	0.313	−0.106
16	**13**	**0.408**	**1.089**	**0.885**	**1.226**	**1.021**	**0.268**	**−0.125**
16	14	0.410	1.090	0.954	1.226	1.090	0.270	−0.122
16	15	0.411	1.091	1.023	1.227	1.159	0.273	−0.120
16	16	0.412	1.091	1.091	1.228	1.228	0.275	−0.118

$$\hat{Q}_{d_{\min}} = \frac{1}{2}\left\{ \hat{r}_{a_1}^2 + \hat{r}_{a_2}^2 \frac{\hat{r}_{p_1}}{\hat{r}_{p_2}} - \hat{r}_{p_1}(\hat{r}_{p_1} + \hat{r}_{p_2}) - \left(1 + \frac{\hat{r}_{p_1}}{\hat{r}_{p_2}}\right)\hat{l}_s^2 \right\}. \tag{20}$$

The amplitude of the flow pulse is then given by

$$\Delta\hat{Q}_d = \hat{Q}_{d_{\max}} - \hat{Q}_{d_{\min}} = \frac{1}{2}\left(1 + \frac{\hat{r}_{p_1}}{\hat{r}_{p_2}}\right)\hat{l}_s^2. \tag{21}$$

The average flow rate for one flow pulsation is given by

$$\hat{\bar{Q}}_d = \frac{1}{(\hat{l}_s - \hat{l}_f)}\int_{\hat{l}_f}^{\hat{l}_s} \hat{Q}_d \, d\hat{l} = \frac{1}{2}\left\{ \hat{r}_{a_1}^2 + \hat{r}_{a_2}^2 \frac{\hat{r}_{p_1}}{\hat{r}_{p_2}} - \hat{r}_{p_1}(\hat{r}_{p_1} + \hat{r}_{p_2}) - \hat{k} \right\}, \tag{22}$$

where l_s is the length of action when the mating teeth just touch, and l_f is the length of action that occurs just prior to another set of teeth making contact within the mesh (i.e., when $\theta_1 = 2\pi/N_1$). Both of these dimensions are shown in Fig. 3. Note: the dimension l_f can be (and usually is) negative. In Eq. (22), the term denoted by the symbol k is given explicitly by

$$\hat{k} = \left(1 + \frac{\hat{r}_{p_1}}{\hat{r}_{p_2}}\right)\left(\frac{(\hat{l}_s + \hat{l}_f)^2 - \hat{l}_s \ \hat{l}_f}{3}\right). \tag{23}$$

Pump Design

In this study, pumps with different numbers of gear teeth are designed for the purposes of comparing flow ripple characteristics. To make an apple-to-apple comparison between pumps, the average flow rate of each pump is maintained as a prescribed constant in the design process. In other words, Eq. (22) is held constant for all pump designs. In this equation, the starting and final length of action (l_s and l_f) is needed to make this computation. The starting length of action is explicitly given in Eq. (12). The final length of action may be determined from the general form of Eq. (15) as

$$\hat{l}_f = \hat{\rho}_{1_f}\sin(\xi - \theta_{1_f} - \beta_{1_f})\sec(\alpha), \tag{24}$$

where

$$\hat{\rho}_{1_f} = \sec(\alpha + \beta_{1_f} + \theta_{1_f} - \xi), \quad \beta_{1_f} = \psi_1 - \sqrt{\hat{\rho}_{1_f}^2 - 1} + \cos^{-1}\left(\frac{1}{\hat{\rho}_{1_f}}\right),$$

$$\theta_{1_f} = \frac{2\pi}{N_1}, \quad \psi_1 = \frac{\pi}{2N_1}, \tag{25}$$

and ξ is given in Eq. (14). The pitch radius of each gear is determined from the following geometry requirements:

$$\hat{r}_{p_1} = \sec(\alpha), \quad \hat{r}_{p_2} = \frac{N_2}{N_1}\hat{r}_{p_1}, \tag{26}$$

where N_1 is the number of teeth on the driving gear and N_2 is the number of teeth on the driven gear. The addendum radius of each gear is designed according the American Gear Manufacturing Association (AGMA) recommended standards [10]. These recommendations are given by

$$\hat{r}_{a_1} = (2 + N_1)\frac{\hat{r}_{p_1}}{N_1}, \quad \hat{r}_{a_2} = (2 + N_2)\frac{\hat{r}_{p_2}}{N_2}. \tag{27}$$

By selecting the number of teeth on each gear (N_1 and N_2), specifying the average flow rate of the pump (Eq. (22)), and enforcing the constraints of Eqs. (24)–(27), the pressure angle α may be solved for numerically. This method has been used to generate the designs that are shown in Table 1.

Figure 5 shows the boldface-row designs given in Table 1. It is interesting to observe that as the number of teeth on the driving gear increases, the teeth become more pointed and sharp at the tip. Furthermore, it is also significant to observe that as the number of teeth on the driven gear decreases, the physical pump size gets smaller while maintaining the same volumetric displacement per revolution.

Results

Center Distance and Physical Pump Size. As shown in Fig. 1, the center distance is the distance between the shaft centerlines of the gears. From geometry, this distance is given by

$$\hat{C} = \hat{r}_{p_1} + \hat{r}_{p_2}, \tag{28}$$

where r_{p_1} and r_{p_2} are the pitch radii of the driving and driven gear, respectively. The center distance can be used to gauge the physical size of the pump. Generally speaking, if the center distance is large, the pump will be large. If the center distance is small, the pump will be small. While designing the pumps for this research, it was observed that the center distance increases strongly as the number of teeth on the driven gear increases and decreases weakly as the number of teeth on the driving gear increases. This result says that physically smaller pumps (of the same displacement per revolution) may be designed if the number of teeth on the driven gear is decreased while the number of teeth on the driving gear is increased. A qualitative assessment of Fig. 5 shows that this is indeed the case. Figure 6 shows a plot of the center distance as it varies with tooth number on both the driving and driven gears. Note: Figure 6 plots the center distance in dimensionless form. To dimensionalize this quantity, it must be multiplied by the radius of the base circle on the driving gear, r_{b_1}.

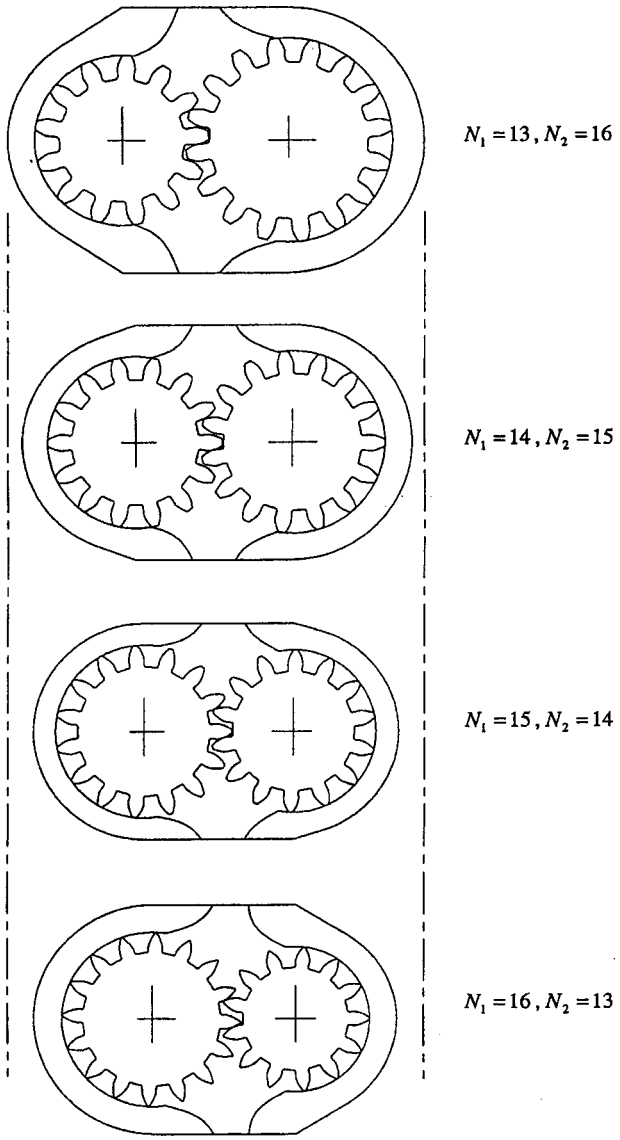

Fig. 5 Gear pumps of the same displacement designed with different numbers of teeth on the driving and driven gears

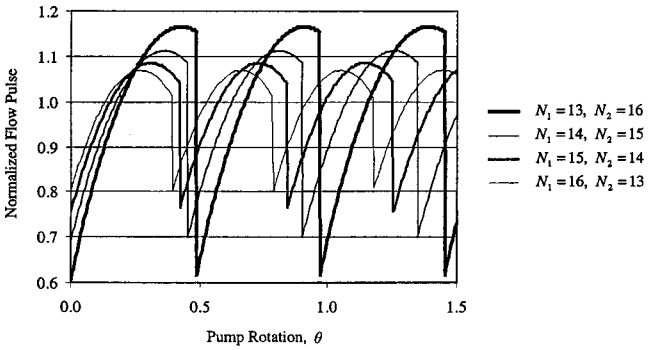

Fig. 7 The theoretical flow pulse solution (Eq. (7)) for the pumps shown in Fig. 5. (Note: these results have been normalized using the average flow rate of the pump. As the number of teeth on the driving gear increases, the flow pulse amplitude is reduced.)

Instantaneous Flow Ripple. The instantaneous flow ripple of the pump is given by the solution to Eq. (7). This solution may be determined by solving for the length of action numerically, as in Eq. (15), or it may be determined using the closed-form approximations for the length of action, as presented in Eq. (17). Figure 7 shows a plot of the flow ripple calculation for the pumps that are shown in Fig. 5. From this figure, it can be seen that the amplitude of the flow ripple decreases significantly as the number of teeth on the driving gear increases. Note: these results are numerical results; however, the approximate closed-form results yield extremely close solutions as well.

Flow Pulse Amplitude. The amplitude of the flow pulse is given by Eq. (21). Figure 8 shows a graph of the flow pulse amplitude as it varies with the numbers of teeth on both the driving and driven gears (i.e., gear 1 and gear 2, respectively). Note: this figure shows a strong dependence on the number of teeth on the driving gear. The flatness of the curves tends to show a weak dependence on the number of teeth on the driven gear.

FFT Results. The fast Fourier transform (FFT) is used to identify the amplitudes and frequencies of the harmonic signals that may be added together to create the flow pulse results that are typically shown in Fig. 7. FFT analysis was conducted on the flow pulse signal that was generated for each pump design in this study. Note: the numerical results were used to conduct this analysis as opposed to the closed-form approximation. Figure 9 shows a comparison of these results for gear sets with equal numbers of teeth on each gear. Figures 10–13 show a comparison of FFT results for gears with differing numbers of teeth on each gear. The frequency

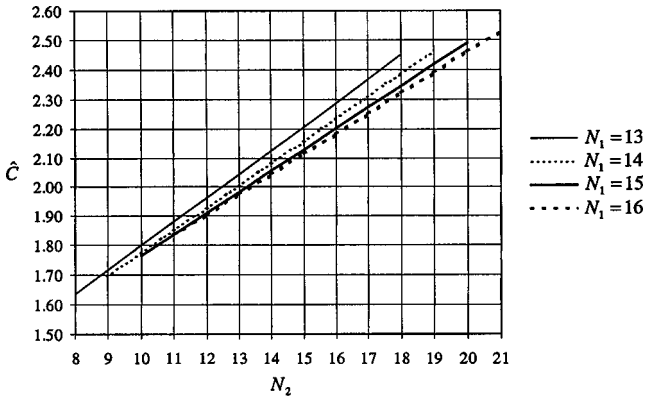

Fig. 6 Dimensionless center distance variation for gear pumps of the same displacement utilizing various combinations of teeth on the driving and driven gears

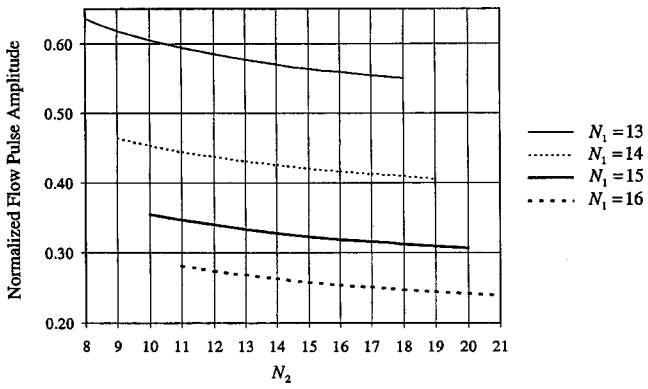

Fig. 8 The theoretical flow pulse amplitude (Eq. (21)) normalized by the average flow rate of the pump. As the number of teeth on the driving gear increases, the flow pulse amplitude is reduced.

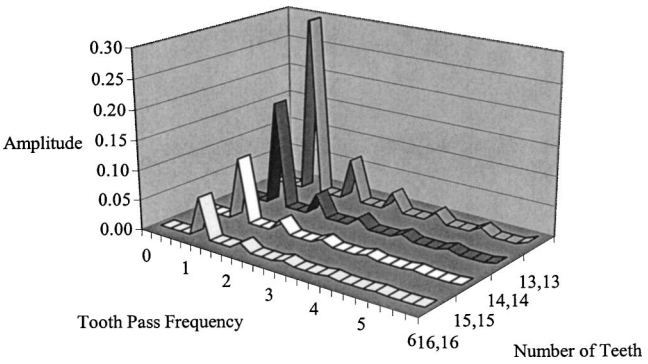

Fig. 9 FFT results for the flow pulse of pumps with equal numbers of teeth on the driving and driven gear

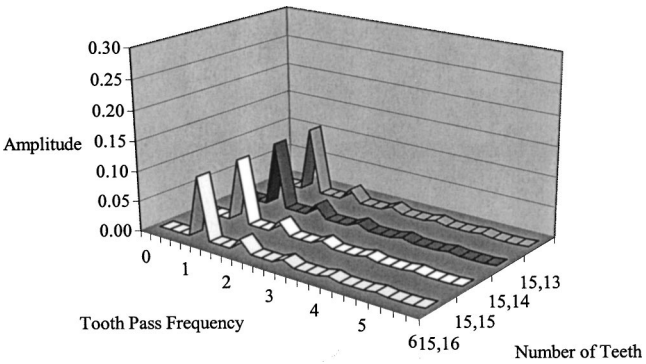

Fig. 12 FFT results for the flow pulse of pumps with 15 teeth on the driving gear 13 to 16 teeth on the driven gear

scale of these plots is normalized by the tooth pass frequency of the driving gear. This normalizing frequency is given by

$$\omega_t = \frac{N_1}{2\pi}\omega_1, \tag{29}$$

where N_1 is the number of teeth on the driving gear and ω_1 is the angular velocity of the driving gear. In Figs. 9–13, tooth numbers are the gears are designated by N_1, N_2. For example, tooth numbers designated by 15, 14 indicate that there are 15 teeth on the driving gear and 14 teeth on the driven gear. This convention is used throughout this paper.

Discussion

As shown in Fig. 6, the center distance between the gear shafts decreases dramatically as the number of teeth on the driven gear goes down. Indeed, Fig. 5 bears this quality as well. From Fig. 6, it may also be observed that a slight decrease in the center distance may be achieved if the number of teeth on the driving gear goes up. This trend suggests that a smaller pump (with the same average flow rate) may be designed if the number of teeth on the driven gear is reduced compared to the number of teeth on the driving gear. For designs of this type, the driven gear will rotate faster than the driving gear according to the speed ratio that characterizes the gearset (i.e., the ratio of teeth). From a packaging point of view, this is a very useful result that may be used to create a smaller machine so long as an unacceptable increase in the flow ripple does not occur. Fortunately, as we have shown already, the amplitude of the flow ripple is fairly insensitive to the number of teeth on the driven gear (see Fig. 8). Therefore, a reduction in the number of teeth on the driven gear, for the purposes of reducing the physical pump size, may be a feasible design alternative that ought to be examined carefully.

Figure 8 shows that the flow-pulse amplitude is significantly reduced by increasing the number of teeth on the driving gear of the pump. It is also shown that increasing the number of teeth on the driven gear can reduce the pulse amplitude only slightly. This characteristic is shown by the flatness of the curves in Fig. 8. The insensitivity of the flow pulse amplitude to the number of teeth on the driven gear is not an obvious result; however, it is one that can be used to one's advantage for making a smaller pump as discussed in the previous paragraph. The FFT results of this study confirm the findings presented in Fig. 8 as well.

The FFT results of Figs. 9–13 show that the harmonic frequencies of the pump occur at integer multiples of the tooth pass frequency of the driving gear. The number of teeth on the driving gear also predominantly controls the amplitude of the harmonic components. As the number of teeth on the driving gear increases, the amplitude of these harmonic components decreases signifi-

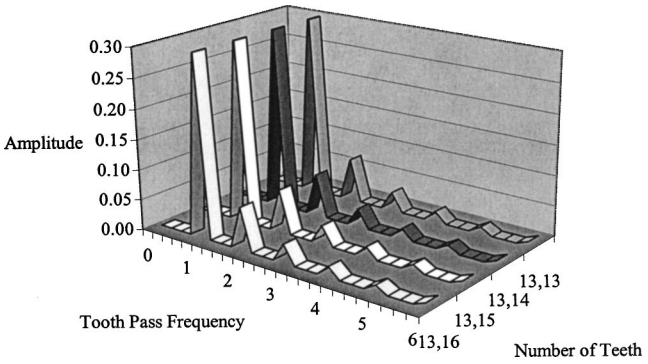

Fig. 10 FFT results for the flow pulse of pumps with 13 teeth on the driving gear 13 to 16 teeth on the driven gear

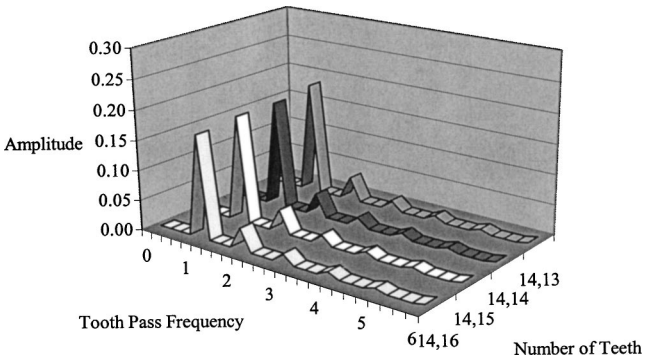

Fig. 11 FFT results for the flow pulse of pumps with 14 teeth on the driving gear 13 to 16 teeth on the driven gear

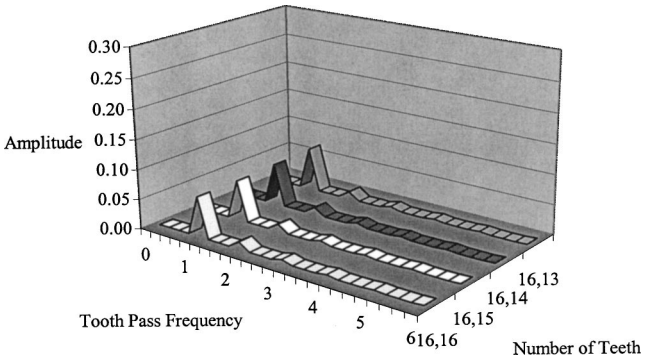

Fig. 13 FFT results for the flow pulse of pumps with 16 teeth on the driving gear 13 to 16 teeth on the driven gear

cantly. As the number of teeth on the driven gear increases, the amplitude of each harmonic component is only decreased slightly. This result is in basic agreement with the previous information presented in Fig. 8.

Conclusion

The following conclusions are supported by the analysis and results of this research:

1. To solve the instantaneous flow ripple equation of the gear pump, a numerical solution is generally required.
2. A closed-form approximation for the flow ripple equation can be used without introducing significant error into the solution. Therefore, Eqs. (7) and (17) may be used for quick calculations that do not require a computer for the solutions.
3. Reducing the numbers of teeth on the driven gear may be used to reduce the center distance and physical pump size. This can be done without altering the average flow rate of the pump and without increasing the flow pulsation dramatically.
4. The center distance can be reduced slightly by increasing the number of teeth on the driving gear as well; however, this impact is not as significant as the one noted in item 3.
5. The pulse amplitude of the flow ripple is primarily determined by the number of teeth on the driving gear of the pump. By increasing the number of teeth on the driving gear, the flow pulse amplitude can be significantly reduced.
6. Increasing the number of teeth on the driven gear can also reduce the pulse amplitude of the flow ripple; however, this impact is not as significant as the one noted in item 5.
7. The harmonic frequencies of the flow ripple pulse occur at integer multiples of the tooth pass frequency on the driving gear; therefore, by increasing the number of teeth on the driving gear, the harmonic frequencies may be increased as well.
8. The number of teeth on the driving gear primarily controls the amplitude of the harmonic components of the flow ripple pulse. As the number of teeth on the driving gear increases, the harmonic amplitudes decrease. This conclusion is in basic agreement with item 5.
9. Changing the number of teeth on the driven gear has a negligible impact on the harmonic amplitudes of the flow ripple pulse. This conclusion is in basic agreement with item 6.

In summary, the results of this study show that it may be advantageous to design an external gear pump with a large number of teeth on the driving gear and a fewer number of teeth on the driven gear. This design configuration will tend to reduce both the physical pump size (without reducing the volumetric displacement of the pump) and the amplitude of the flow pulsation, while increasing the natural harmonic frequencies of the machine.

ACKNOWLEDGMENT

The authors would like to thank Haldex Burnes and the Fluid Power Research Consortium at the University of Missouri, Columbia, for many helpful discussions and for their support of this work.

Nomenclature

C = center distance between shafts on the gear pump
k = pump constant used for defining the average volumetric flow rate
l = instantaneous length of action within the gear mesh
l_f = length of action within the gear mesh just prior to another set of teeth making contact
l_s = length of action within the gear mesh when the teeth make the first point of contact
$N_{1,2}$ = number of teeth on the driving and driven gear
Q = volumetric flow rate
Q_d = volumetric discharge flow rate of the pump
$\overline{Q}_d$ = average volumetric flow rate of the pump

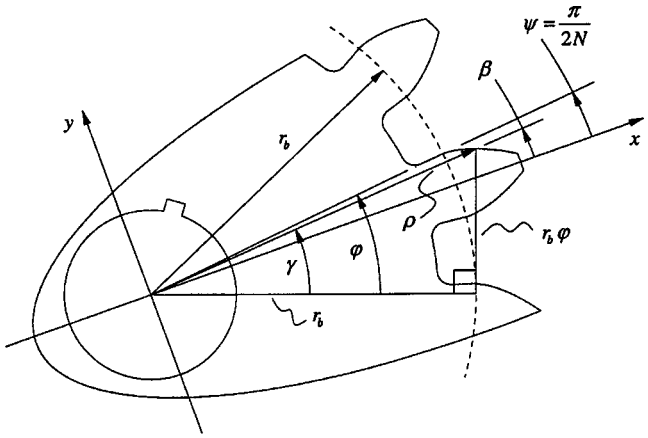

Fig. 14 The geometry of the involute tooth profile

$Q_{d_{\max}}$ = maximum volumetric flow rate of the pump
$Q_{d_{\min}}$ = minimum volumetric flow rate of the pump
ΔQ_d = amplitude of the volumetric flow rate pulse
r = radial dimension
$r_{a_{1,2}}$ = addendum radius of the driving and driven gear
$r_{b_{1,2}}$ = base circle radius of the driving and driven gear
$r_{p_{1,2}}$ = pitch radius of the driving gear
t = time
V = volume
V_d = volume leaving the control volume across the discharge boundary
$V_{i_{1,2}}$ = volume entering the control volume with the driving and driven gear
$V_{o_{1,2}}$ = volume leaving the control volume with the driving and driven gear
w = width of the gear teeth
x = primary Cartesian coordinate
y = secondary Cartesian coordinate
α = pressure angle
$\beta_{1,2}$ = angular dimension locating the instantaneous point of contact on the driving and driven gear
β_{1_f} = angular dimension locating the point of contact on the driving gear just prior to another set of teeth making contact
β_{1_s} = angular dimension locating the point of contact on the driving gear when the teeth make the first point of contact
$\theta_{1,2}$ = angular displacement of the driving and driven gear
θ_{1_f} = angular displacement of the driving gear just prior to another set of teeth making contact
ξ = angular orientation of the fixed Cartesian coordinate system
ρ = radial dimension
$\rho_{1,2}$ = radial dimension locating the instantaneous point of contact on the driving and driven gear
ρ_{1_f} = radial dimension locating the point of contact on the driving gear just prior to another set of teeth making contact
ρ_{1_s} = radial dimension locating the point of contact on the driving gear when the teeth make the first point of contact
ψ_1 = half angle of the tooth width measured at the base circle of the driving gear
$\omega_{1,2}$ = angular velocity of the driving and driven gear
ω_t = tooth pass frequency of the driving gear

Appendix

In this Appendix, the geometry of the involute tooth profile is presented. Figure 14 shows the involute geometry that defines the surface profile of a single gear tooth. A well-known method for visualizing the involute profile is to generate a curve by unwrapping a tight string from the outside edge of a cylinder. In Fig. 14, the outside edge of this cylinder is defined by the radius of the base circle, r_b, and the unwrapped length of the tight string is given by the arc length $r_b\ \varphi$. A point on the involute surface of the tooth is located by the polar coordinates ρ and β. This point also has Cartesian coordinates given by x and y. Note the x axis is located along the centerline of the tooth. From the geometry of right triangles, the following results can be written for the polar coordinates of a point located on the involute surface:

$$\rho = r_b\sqrt{1+\varphi^2}, \quad \beta = \psi - \varphi + \gamma, \tag{30}$$

where ψ is a fixed geometry parameter of the tooth, φ is called the involute angle, and γ is the acute angle of the right triangle shown in Fig. 14. The Cartesian transformation of these coordinates is given by

$$x = \rho\cos(\beta), \quad y = \rho\sin(\beta). \tag{31}$$

From the geometry of Fig. 14, it may also be observed that

$$r_b = \rho\cos(\gamma), \quad r_b\varphi = \rho\sin(\gamma). \tag{32}$$

Using Eqs. (30) and (32), it can be shown that

$$\beta = \psi - \sqrt{\left(\frac{\rho}{r_b}\right)^2 - 1} + \cos^{-1}\left(\frac{r_b}{\rho}\right). \tag{33}$$

These geometry relationships are referred to and used throughout the analysis of this research.

References

[1] Frith, R. H., and Scott, W., 1996, ''Comparison of an external gear pump wear model with test data,'' Wear, **196**, pp. 64–71.

[2] Koc, E., and Hooke, C. J., 1997, ''An experimental investigation into the design and performance of hydrostatically loaded floating wear plates in gear pumps,'' Wear, **209**, pp. 184–192.

[3] Koc, E., 1994, ''Bearing misalignment effects on the hydrostatic and hydrodynamic behaviour of gears in fixed clearance end plates,'' Wear, **173**, pp. 199–206.

[4] Koc, E., 1991, ''An investigation into the performance of hydrostatically loaded end-plates in high pressure pumps and motors: Movable plate design,'' Wear, **141**, pp. 249–265.

[5] Foster, K., Taylor, R., and Bidhendi, I. M., 1985, ''Computer prediction of cyclic excitation sources for an external gear pump,'' Proc. Inst. Mech. Eng., Part C: Mech. Eng. Sci., **199**, No. B3, pp. 175–180.

[6] Chen, C. K., and Yang, S. C., 2000, ''Geometric modeling for cylindrical and helical gear pumps with circular arc teeth,'' Proc. Inst. Mech. Eng., Part C: J. Mech. Eng. Sci., **214**, pp. 599–607.

[7] Mitome, K., and Seki, K., 1983, ''A new continuous contact low-noise gear pump,'' Journal of Mechanisms, Transmission and Automation in Design, **105**, pp. 736–741.

[8] Manring, N. D., 2000, ''The discharge flow ripple of an axial-piston swash-plate type hydrostatic pump,'' ASME J. Dyn. Syst., Meas., Control, **122**, pp. 263–268.

[9] Ivantysyn, J., and Ivantysynova, M., 2001, *Hydrostatic Pumps and Motors*, Akademia Books International, New Delhi.

[10] Norton, R. L., 2000, *Machine Design—An Integrated Approach*, 2nd ed., Prentice-Hall, Inc., Upper Saddle River, NJ.